CHEMISTRY OF MATERIALS
Cite This: Chem. Mater. 2019, 31, 5890−5899
Article
pubs.acs.org/cm

Combined Theoretical and Experimental Investigations of Atomic Doping To Enhance Photon Absorption and Carrier Transport of $LaFeO_3$ Photocathodes

Garrett P. Wheeler,[†,∥] Valentin Urena Baltazar,[‡,∥] Tyler J. Smart,[‡] Andjela Radmilovic,[†] Yuan Ping,*[,§] and Kyoung-Shin Choi*[,†]

[†]Department of Chemistry, University of Wisconsin, Madison, Wisconsin 53706, United States
[‡]Department of Physics and [§]Department of Chemistry and Biochemistry, University of California, Santa Cruz, California 95064, United States

Supporting Information

ABSTRACT: Perovskite-type lanthanum iron oxide, $LaFeO_3$, is a p-type semiconductor that can achieve overall water splitting using visible light while maintaining photostability. These features make $LaFeO_3$ a promising photocathode candidate for various photoelectrochemical cells. Currently, the photoelectrochemical performance of a $LaFeO_3$ photocathode is mainly limited by considerable bulk electron−hole recombination. This study reports a combined theoretical and experimental investigation on the atomic doping of $LaFeO_3$, in particular, substitutional doping of La^{3+} with K^+, to increase its charge-transport properties and decrease electron−hole recombination. The computational results show that K-doping enhances not only the charge-transport properties but also photon absorption below the bandgap energy of the pristine $LaFeO_3$. The effect of K-doping was systematically investigated by comparing the electronic and atomic structures, majority carrier density, hole-polaron formation, and optical properties of pristine and K-doped $LaFeO_3$. The computational results were then verified by experimentally characterizing the crystal structures, compositions, optical properties, and photoelectrochemical properties of $LaFeO_3$ and K-doped $LaFeO_3$ electrodes. For this purpose, pristine $LaFeO_3$ and K-doped $LaFeO_3$ were prepared as high-surface-area, high-purity photoelectrodes having the same morphology to accurately and unambiguously evaluate the effect of K-doping. The combined computational and experimental investigations presented in this study provide useful insights into the effect of composition tuning of $LaFeO_3$ and other p-type oxides with a perovskite structure.

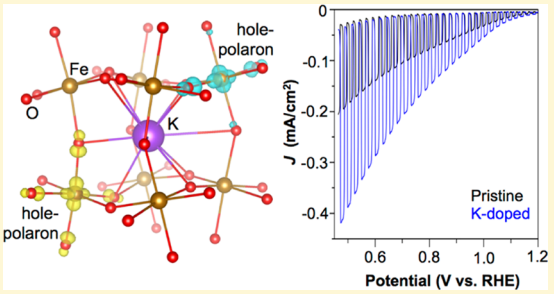

INTRODUCTION

Perovskite-type lanthanum iron oxide, $LaFeO_3$, is a p-type semiconductor that can achieve overall water splitting using visible light; its bandgap energy is 2.1−2.2 eV, and its conduction band minimum (CBM) and valence band maximum (VBM) straddle the water reduction and oxidation potentials.[1−4] Furthermore, $LaFeO_3$ is reported to be stable against photocorrosion,[1] which is a significant advantage over Cu-containing oxide photocathodes that are typically unstable during photocurrent generation.[5−8] These features make $LaFeO_3$ a very promising photocathode candidate for a photoelectrochemical cell (PEC) used for water splitting or other solar fuel production (e.g., CO_2 reduction and N_2 reduction). However, studies on $LaFeO_3$ for use as a photocathode have been very limited to date.[1,2,9,10] The major limitation of a $LaFeO_3$ photocathode appears to be considerable bulk electron−hole recombination, judging from the fact that the highest photocurrent generated by $LaFeO_3$ to date even for O_2 reduction,[1] which has much faster reduction kinetics than water reduction on the $LaFeO_3$ surface,[1,11,12] is still significantly lower than the theoretically expected photocurrent based on its bandgap energy.[13,14]

One straightforward strategy that has been effective to improve charge-transport properties and bulk electron−hole separation in oxide-based photoelectrodes is to increase the majority carrier density through atomic doping.[5,13,15,16] In this study, we conducted computational and experimental studies to investigate K-doping at the La site of $LaFeO_3$, which resulted in an increase not only in carrier density but also in photon absorption. Although there have been a few studies on the doping of $LaFeO_3$ at the La site, the focus of these studies was not to investigate $LaFeO_3$ as a semiconductor photocathode but to investigate it as an ion conductor or catalyst.[17−20] Therefore, the effect of doping at the La site relevant to the photoelectrochemical properties of $LaFeO_3$ such as photon absorption and carrier transport has not been elucidated prior to this study.

Received: May 31, 2019
Revised: July 1, 2019
Published: July 16, 2019

DOI: 10.1021/acs.chemmater.9b02141
Chem. Mater. 2019, 31, 5890−5899

In this study, we first report the computational results that systematically determined the effect of K-doping on the electronic and atomic structures, majority carrier density, hole-polaron formation, and optical properties of $LaFeO_3$. Then, we report experimental results and compare them with the computational results. For our experimental studies, $LaFeO_3$ and K-doped $LaFeO_3$ were prepared as high-surface-area, high-purity photoelectrodes having the same morphology to accurately and unambiguously evaluate the effect of K-doping. The combined computational and experimental investigations presented in this study will provide useful insights into the effect of composition tuning of $LaFeO_3$ that may be applied to the composition tuning of other p-type oxides with a perovskite structure to enhance their photoelectrochemical properties.

EXPERIMENTAL SECTION

Computational Methods. *Electronic Structure.* Density functional theory calculations were performed using the Quantum ESPRESSO package[21] with PBE + U exchange and correlation functional, with a Hubbard U parameter on O 2p of 2 eV and Fe 3d of 3 eV and norm-conserving pseudopotential[22] with a plane wave energy cutoff of 80 Ry. A total energy convergence of at least 10^{-7} Ry was used for all self-consistent calculations, whereas atomic forces were relaxed until a threshold of 10^{-3} Ry/au was met. Final calculations implemented a 2 × 2 × 2 supercell consisting of 160 atoms with a k-point grid of 2 × 2 × 1 with the cell parameters attained via a variable cell relaxation. To investigate the effect of K-doping, 1 out of 32 La atoms was replaced with a K atom, which is equivalent to 3 atom % K-doping at the La site. This level of doping was chosen for computational studies because experimental studies showed that 3 atom % K-doping at the La site is optimal for enhancing the photoelectrochemical properties of $LaFeO_3$.

Optical Absorption Spectrum. To study the optical absorption of pristine and doped $LaFeO_3$, we computed the imaginary part of the dielectric function in the random phase approximation with local field effects, as implemented in the YAMBO code.[23] The input of this calculation came directly from our single-particle eigenvalues and wavefunctions from DFT + U computed in Quantum ESPRESSO.[21] To directly compare with experimental results, we computed the absorption spectra (α) directly from the real and imaginary parts of dielectric function (ϵ_1 and ϵ_2, respectively) using the equation below.[24]

$$\alpha(\omega) = \frac{\omega}{c}\frac{\epsilon_2(\omega)}{\sqrt{\frac{\epsilon_1(\omega) + \sqrt{\epsilon_1(\omega)^2 + \epsilon_2(\omega)^2}}{2}}}$$

Experimental Methods. *Materials.* Lanthanum(III) nitrate ($La(NO_3)_3{\cdot}6H_2O$, 99.99%) was purchased from Chem-Impex Int'l Inc. Iron(II) chloride ($FeCl_2{\cdot}4H_2O$, 98%) and propylene carbonate ($CH_3C_2H_3O_2CO$, 99%) were purchased from Alfa-Aesar. Potassium nitrate (KNO_3, 99%) and potassium hydroxide (KOH, ≥85%) were purchased from Sigma-Aldrich. Fluorine-doped tin oxide (FTO) on glass was used as the substrate for electrodeposition and was purchased from Hartford Glass Co. All aqueous solutions were prepared using deionized (DI) water with a resistivity of 18.2 MΩ cm. Substrates were cleaned by sonication in methanol, isopropyl alcohol, and DI water (10 min each) to ensure a clean deposition surface. All chemicals were used as purchased without further purification.

Synthesis of Pristine and K-Doped $LaFeO_3$ Electrodes. Co-electrodeposition of $La(OH)_3$ and $Fe(OH)_2$ was carried out in an undivided cell using a VMP2 multichannel potentiostat (Princeton Applied Research). A typical three-electrode system composed of an FTO working electrode (WE), a Ag/AgCl (4 M KCl) reference electrode, and a Pt counter electrode was used. The Pt counter electrode was prepared by sputter coating 20 nm of titanium followed by 100 nm of platinum onto a clean glass slide. The FTO working electrode was masked with an insulating tape (3 M, electroplating tape 470) to expose a circular geometric area of 0.5 cm^2. This eliminated any edge effects and ensured uniformity of the deposited film.[25]

To prepare a pristine $LaFeO_3$ film, a precursor film composed of a 1:1 ratio of $La(OH)_3$ and $Fe(OH)_2$ was deposited using an aqueous solution containing 21 mM $La(NO_3)_3{\cdot}6H_2O$, 18 mM $FeCl_2{\cdot}4H_2O$, and 400 mM KNO_3 as the plating solution.[1] The La/Fe ratio in the as-deposited films was confirmed to be 1:1 using energy dispersive X-ray spectroscopy (EDS). For K-doped $LaFeO_3$ films, the amount of $La(NO_3)_3$ precursor was systematically decreased to obtain a desired $1 - x$:1 ratio of $La(OH)_3$ and $Fe(OH)_2$. The deposition procedure consisted of applying a constant current (galvanostatic) pulse with a current density of −3.8 mA/cm^2 passing 0.1 C/cm^2 followed by a 30 s rest. Three pulses were applied so that a total charge of 0.3 C/cm^2 was passed. The potential applied to the WE at the end of each galvanostatic pulse was between 1.12 and 1.15 V vs Ag/AgCl. During the galvanostatic pulse, nitrate reduction occurred at the WE to cause an increase in local pH,[26] which resulted in the co-precipitation of $La(OH)_3$ and $Fe(OH)_2$ onto the FTO working electrode. During the resting time between pulses, the nitrate, La^{3+}, and Fe^{2+} ions were replenished at the WE/electrolyte interface. We found that the pulsed deposition sequence with sufficient resting time increased the uniformity of the resulting films. Because $Fe(OH)_2$ is spontaneously oxidized by ambient oxygen to FeOOH, the as-deposited films composed of $La(OH)_3$ and FeOOH were light orange in color.

Pristine $LaFeO_3$ films were obtained by annealing the precursor films at 600 °C for 6 h in the air (ramp rate = 1.66 °C/min). To obtain K-doped $LaFeO_3$ films, the precursor films were annealed with a drop-casted K-containing solution covering the film surface (150 μL/cm^2). The K-containing solutions were prepared by adding 50, 100, or 150 μL of an aqueous 50 mM KNO_3 stock solution to 5 mL of propylene carbonate containing 2 vol % H_2O to make 0.5, 1.0, or 1.5 mM drop-cast solutions, respectively. The K concentrations of the drop-cast solutions and corresponding K content in the K-doped $LaFeO_3$ films as determined by EDS are summarized in Table 1.

Table 1. KNO_3 Drop-Cast Solution Concentrations and Percentages of Potassium in the Annealed $LaFeO_3$ Films

concentration of K in drop-cast solution	atomic % of K in La site of $LaFeO_3$
0.5 mM	1.5%
1.0 mM	3%
1.5 mM	7%

Characterization. The purity and crystallinity of the resulting $LaFeO_3$ electrodes were confirmed by powder X-ray diffraction (XRD, D8 Discover, Bruker, Ni-filtered Cu Kα radiation, λ = 1.5418 Å). The surface morphology and elemental composition were characterized with scanning electron microscopy (SEM; LEO Supra55 VP, an accelerating voltage of 2 kV) and energy dispersive X-ray spectroscopy (EDS; Noran System Seven, Thermo-Fisher, ultra-dry silicon drift detector, an accelerating voltage of 15 kV). Bandgaps were determined from UV−visible−near infrared (UV−vis−NIR) absorption spectra obtained using an integration sphere to collect all reflected and transmitted light from the electrode, allowing for more accurate determination of absorbance (Cary 5000 UV−vis−NIR spectrophotometer, Agilent). X-ray photoelectron spectroscopy (XPS) spectra were measured using a K-Alpha X-ray photoelectron spectrometer (Thermo Scientific) equipped with Al Kα excitation. The binding energies were calibrated with respect to the carbon 1s peak at 284.8 eV.

Photoelectrochemical and Electrochemical Characterization. All photoelectrochemical and electrochemical measurements were carried out using an SP-200 potentiostat/EIS (Bio-Logic Science Instrument). Solar illumination was simulated by filtering light from a 300 W Xe arc lamp through a water IR filter, neutral density filters, and an AM 1.5G filter. The light was then directed to the sample using an

DOI: 10.1021/acs.chemmater.9b02141
Chem. Mater. 2019, 31, 5890−5899

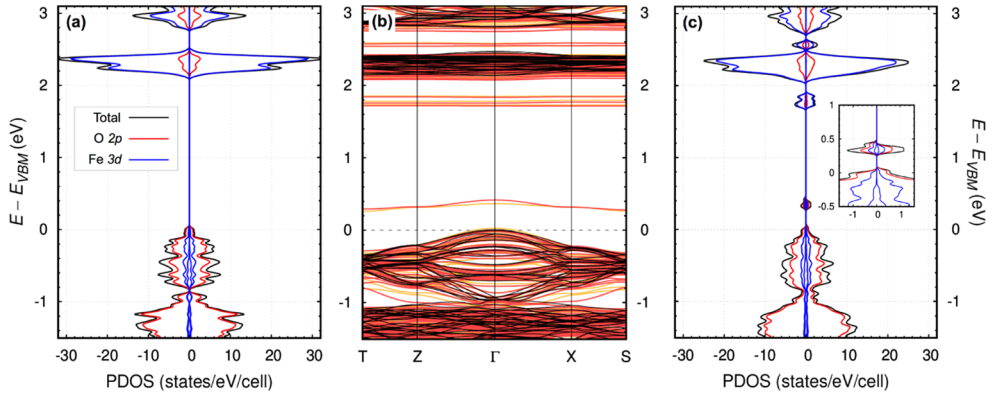

Figure 1. (a) Total (black) and projected (red for O 2p and blue for Fe 3d) density of states of pristine $LaFeO_3$. The reference zero is chosen to be at the valence band maximum. (b) Band structure of pristine (black) and K-doped $LaFeO_3$ (red = spin up and orange = spin down). (c) Total (black) and projected (red for O 2p and blue for Fe 3d) density of states of K-doped $LaFeO_3$. The inset image shows magnified hole-polaron states.

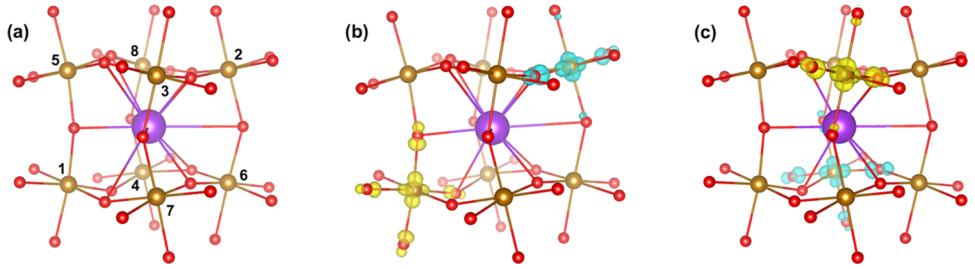

Figure 2. (a) Cube composed of eight Fe atoms at the corners numbered from 1 through 8 with a K atom at the center (K = purple, Fe = brown, O = red). (b, c) Hole-polaron wavefunction modulus with an isosurface at 10% of the maximum value for the spin up (yellow) and spin down (turquoise); (b) hole-polarons formed at the (1, 2) Fe pair, which are symmetrically identical to those formed at the (5, 6) Fe pair; (c) hole-polarons formed at the (3, 4) Fe pair, which are symmetrically identical to those formed at the (7, 8) Fe pair.

optical fiber. The light source was calibrated to 100 mW/cm^2 (1 sun) using an NREL-certified Si reference cell (Photo Emission Tech. Inc.). The working electrode was masked with resin to make the exposed geometrical area (ca. 0.02−0.03 cm^2) smaller than the illuminated area (0.06 cm^2). Illumination of the working electrode was through the FTO contact (back-side illumination). An undivided three-electrode cell composed of a working electrode ($LaFeO_3$), a Pt counter electrode, and a Ag/AgCl (4 M KCl) reference electrode was used.

J−*V* plots were obtained under chopped illumination by sweeping the potential to the negative direction with a scan rate of 10 mV/s (for O_2 reduction) or 5 mV/s (for water reduction). A slower scan rate was chosen for water reduction to allow transient photocurrent to further stabilize within the "light-on" duration of chopped illumination. *J*−*t* plots were obtained by applying a constant potential. All measurements were performed in a 0.1 M KOH solution (pH 13) while continuously bubbling N_2 (for water reduction) or O_2 (for O_2 reduction) and stirring rapidly. For testing water reduction, a custom-built, airtight three-electrode cell using a thinner Ag/AgCl (3 M NaCl) reference was employed. The cell and the solution were thoroughly purged with N_2 before photocurrent measurements. During photocurrent measurement, N_2 was constantly purged in the solution through a gas inlet and an outlet of the cell, preventing the presence of O_2 in the cell. Although a Ag/AgCl reference electrode was used to monitor the system, all results in this work are presented against the reversible hydrogen electrode (RHE) for easy comparison with other reports that used electrolytes with different pH conditions. The conversion between potentials vs Ag/AgCl and vs RHE is performed using the equation below.

$$E(\text{vs RHE}) = E(\text{vs Ag/AgCl}) + E_{\text{Ag/AgCl}}(\text{reference}) + 0.0591\ \text{V} \times \text{pH}$$

($E_{\text{Ag/AgCl}}$(reference, 4M KCl) = 0.1976 V vs NHE at 25°C)

($E_{\text{Ag/AgCl}}$(reference, 3M NaCl) = 0.209 V vs NHE at 25°C)

Incident photon-to-current efficiency (IPCE) at each wavelength was measured using AM 1.5G illumination from a 150 W Xe arc lamp. Monochromatic light was generated by using an Oriel Cornerstone 130 monochromator with a 10 nm bandpass, and the output was measured with a photodiode detector. IPCE was measured at 0.65 V vs RHE in 0.1 M KOH (pH 13) with continuous O_2 bubbling. The same three-electrode setup was used for the oxygen reduction photocurrent measurement as for the water reduction measurement. Absorbed photon-to-current efficiency (APCE) was obtained by dividing the IPCE by the light harvesting efficiency (LHE) at each wavelength using the equations below.

$$\text{APCE}\ (\%) = \text{IPCE}\ (\%)/\text{LHE}$$

$$\text{LHE} = 1 - 10^{-A(\lambda)}\ (A(\lambda)\text{: absorbance at wavelength } \lambda)$$

Capacitance measurements for Mott−Schottky plots were obtained using a typical three-electrode system composed of a masked $LaFeO_3$ working electrode with an exposed surface area of ~0.08 cm^2, a Pt counter electrode, and a Ag/AgCl (4 M KCl) reference electrode. A 0.1 M KOH solution (pH 13) was used. A sinusoidal modulation of 10 mV was applied at frequencies of 0.5 and 1 kHz. Further details of the photoelectrochemical and electrochemical characterizations can be found elsewhere.[25]

RESULTS AND DISCUSSION

Computational Studies. *Effect of K-Doping on Electronic Structure and Optical Absorption.* $LaFeO_3$ is a charge-transfer insulator with valence states mainly composed of O 2p and conduction states mainly composed of Fe 3d orbitals (Figure 1a). The electronic band structure of pristine $LaFeO_3$ shows a direct Γ−Γ bandgap of 2.13 eV. We used Hubbard *U*

DOI: 10.1021/acs.chemmater.9b02141
Chem. Mater. 2019, 31, 5890−5899

parameters of 2 eV for O 2p and 3 eV for Fe 3d, which enables the formation of both electron- and hole-polarons and results in a bandgap value of pristine $LaFeO_3$ close to the reported experimental value.[1] We confirmed that the major effects of K-doping on the band structure of $LaFeO_3$ discussed here are not affected by the choice of U parameters as long as they are chosen to allow for the formation of both electron- and hole-polarons.[15,27−29] For example, the major results obtained with Hubbard U parameters of 4 eV for O 2p and 5 eV for Fe 3d (Figure S1) are the same as those shown in Figure 1, although the exact energy levels of the band structures may vary.

After doping the system with K, we observed the formation of an isolated hole-polaron state, which is a hybridized state consisting of O 2p and Fe $3d_{x^2-y^2}$ located at 0.3 eV above the VBM (Figure 1b,c). This suggests that the two holes generated by the replacement of La^{3+} with K^+ are localized on Fe atoms and their neighboring O atoms,[30] forming Fe^{4+}. This result agrees well with experimental observations that the electrical conduction and dipolar relaxation in $LaFeO_3$ are dominated by polaronic hole hopping between Fe^{4+} and Fe^{3+}.[31,32] Figure 2a shows a structural unit of $LaFeO_3$ where eight Fe atoms numbered 1 through 8 are located at the corners of a cube with a K atom at the center. The most energetically preferred configurations of the two hole-polarons formed by K-doping are those with the holes occupying Fe at the off-diagonal corners. Due to crystal symmetry, only two unique Fe−Fe diagonal positions are present, as shown in Figure 2b,c (Table S1). Between these two configurations, the one shown in Figure 2b is more stable by 113 meV. Considering that our calculations were performed at 0 K and only included electronic energy without an entropy contribution, it is possible that a non-negligible concentration of hole-polarons formed in the sample at room temperature may exist in the configuration shown in Figure 2c.

Our calculations also showed that K-doping decreases the bandgap by lowering the conduction band minimum (CBM) from 2.13 to 2.06 eV and additionally forms multiple highly localized states below the CBM (Figure 1b,c). We note that these states are formed not due to the presence of K but due to the free holes from K-doping that form small polarons, which perturbed the system. (Even when free holes are introduced without K, the same states form.)

To understand how these changes in the electronic structure affect the optical properties of the system, we calculated the absorption spectra of pristine and K-doped $LaFeO_3$ (Figure 3). Because of the presence of optical anisotropy in the system, we averaged optical responses from light that was polarized along the a, b, c crystal axes. The results showed that K-doping causes a negligible change in the high-energy range (≥2.4 eV) in terms of the position and intensity of the absorption peaks. However, K-doping clearly enhances absorption in the low-energy range (<2.4 eV) due to the lowering of the CBM and the introduction of perturbed states below the CBM. Since the solar spectrum contains a considerable number of photons near 2 eV,[14] even a small increase in absorbance in this region may significantly increase the number of photons that can be utilized by $LaFeO_3$ for photocurrent generation. We note that we did not include excitonic effects in this calculation because in most transition-metal oxides, the exciton binding energy is small (∼0.1 eV), and its change by doping is negligible.[33−35]

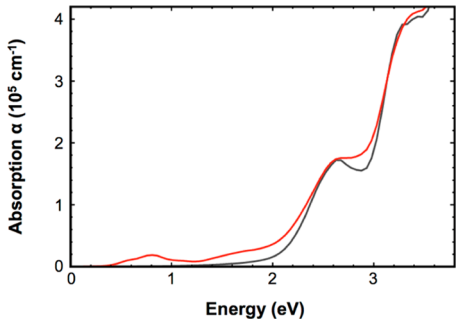

Figure 3. Calculated absorption spectra for pristine (black) and K-doped (red) $LaFeO_3$.

K as a Shallow Acceptor in $LaFeO_3$. Although K-doping introduces two holes into the system, the experimental carrier concentration will only increase when the dopant site does not trap the holes within the system. A dopant is generally considered to be a trap if the defect ionization energy or the energy that is required to free a defect-bound polaron is much higher than kT. We computed the defect ionization energies from first principles. First, we obtained the formation energy of the defect at a charge state q (E_q^f) using the following equation:

$$E_q^f[\varepsilon_F] = E_q - E_{pst} + \sum_i \mu_i \Delta N_i + q\varepsilon_F + \Delta_q$$

where E_q is the total energy of the system with the charged defect, E_{pst} is the total energy of the pristine system, ΔN_i is the change in the number of atoms of element i between pristine and defective systems, and μ_i is the atomic chemical potential of element i in its stable form. Δ_q is the charged defect correction that removes the spurious interactions between charges in periodic images and is computed by the method described in a previous study.[36] Finally, ε_F is the electron chemical potential or Fermi level, which varies from VBM to CBM of the pristine system.

Next, we calculated the charge transition level (CTL), denoted as $\varepsilon^{q/q'}$, which is the value of the Fermi level when the system undergoes a transition from one stable charge state q to another q'. This can be computed by defect formation energies at different charge states using the equation shown below, where $E_q^f[\varepsilon_F = 0]$ is the formation energy of the defect in the charge state q when the Fermi level is at the VBM ($\varepsilon_F = 0$).

$$\varepsilon^{q|q'} = \frac{E_q^f[\varepsilon_F = 0] - E_{q'}^f[\varepsilon_F = 0]}{q' - q}$$

The difference between this CTL and the appropriate band edge corresponds to the defect ionization energies.

In K-doped $LaFeO_3$, the $q = -1$ system (where one of the two holes from K substitution of La has been removed) is unstable leading to a direct $q = 0$ to $q = -2$ transition. Furthermore, the value of this charge transition level ($\varepsilon^{0|-2}$) is only 30 meV above the VBM. Since the energy required for this transition is comparable to kT at room temperature (25 meV), K can serve as a shallow acceptor. We also note that the ionization energy obtained from defect formation energies is not significantly different from the energy difference between the VBM and the position of the hole state in the PDOS (Figure 1c). This result indicates that the DFT + U level has largely corrected the delocalization errors that are known to occur at the semilocal DFT level. Additionally, it implies that the geometry relaxation at different charge states has a minimal contribution.[37,38] From these results, we concluded that K-

DOI: 10.1021/acs.chemmater.9b02141
Chem. Mater. 2019, 31, 5890−5899

doping can effectively increase the hole concentration in $LaFeO_3$.

Effects of K-Doping on Atomic Structure. $LaFeO_3$ has a perovskite structure in which the La atoms are located at the center of a cube composed of eight Fe atoms at the corners that are octahedrally coordinated with O. However, the atoms in $LaFeO_3$ are slightly displaced from those of an ideal cubic perovskite structure, and $LaFeO_3$ has an orthorhombic *Pnma* structure with a G-type antiferromagnetic ordering on the Fe atoms.[39] Theoretically predicted cell parameters for pristine and K-doped $LaFeO_3$ are shown in Table 2. For K-doped $LaFeO_3$, the results for two configurations of hole-polaron formation shown in Figure 2b,c are shown as Configuration 1 and Configuration 2, respectively.

Table 2. Theoretically Predicted Cell Parameters and Bandgap Values for Pristine $LaFeO_3$ and K-Doped $LaFeO_3$

system	a (Å)	b (Å)	c (Å)	volume (Å^3)
pristine	5.652	7.903	5.568	248.69
K-doped (configuration 1)	5.644	7.887	5.569	247.91
K-doped (configuration 2)	5.649	7.886	5.566	247.95

Despite the fact that K^+ (164 pm) has a larger ionic radius than La^{3+} (136 pm),[40] the result shows that K-doping (one K atom in the 160 atom cell) shrinks the unit cell volume by ~0.3% for both configurations. This is because a fraction of Fe^{3+} (64.5 pm) is substituted by Fe^{4+} (58.5 pm) owing to the hole-polaron formation. To confirm this, we considered four different systems: (1) a pristine sample with a neutral charge; (2) a pristine sample plus two holes without K-doping, giving a +2 charge; (3) K-doped minus two holes, giving a −2 charge; and (4) a K-doped sample with corresponding Fe^{4+} formation with a neutral charge (Table S2). System 2 has the same number of Fe^{4+} ions as System 4, but La is not replaced with K. System 3 has no Fe^{4+} formation even though La is replaced with K. We found that System 2 (the pristine sample plus two holes, +2 charge) showed a decreased cell volume due to Fe^{4+} formation, whereas System 3 (the K-doped sample minus two holes, −2 charge) showed an increased cell volume, because K^+ has a larger radius than La^{3+}. System 4 (the K-doped sample with corresponding Fe^{4+} formation) showed consistency with the average cell volume of Systems 2 and 3, as expected. However, because the magnitude of cell shrinkage caused by the formation of Fe^{4+} is greater than that of expansion caused by the replacement of La by K, the cell volume of System 4 is smaller than that of the pristine sample (System 1).

Experimental Studies. The $LaFeO_3$ electrodes used in this study were prepared using a method reported in our previous study.[1] This method is composed of two steps. The first step is electrodeposition of a precursor film composed of $La(OH)_3$ and $Fe(OH)_2$ with a La/Fe ratio of 1:1, which was confirmed by EDS. The second step is thermal annealing of the precursor film at 600 °C in the air, which converts the precursor film to a crystalline $LaFeO_3$ film.

To produce K-doped $LaFeO_3$ films in which K substitutionally replaces La ($La_{1-x}K_xFeO_3$), the precursor film was deposited with a La/Fe ratio of $1 - x$:1. Then, the precursor film was covered with a drop-casted solution containing K^+ and annealed at 600 °C in the air to form $La_{1-x}K_xFeO_3$ films. The drop-cast solution consisted of KNO_3 dissolved in propylene carbonate containing 2 vol % H_2O. The porous precursor film contained air in the void space and could not be easily wetted with an aqueous KNO_3 solution, resulting in nonuniform K incorporation into the film (Figure S2). The use of propylene carbonate allowed for uniform wetting of the precursor film (Figure S2) and, thus, uniform K incorporation into the precursor film during annealing. Elemental mapping EDS of a representative film that shows the even distribution of K throughout the film is shown in Figure S3.

Among the K-doped $LaFeO_3$ films prepared with 1.5, 3, and 7 atom % K at the La site, the 3 atom % K-doped $LaFeO_3$ was identified to contain an optimal amount of K dopant in terms of enhancing photocurrent generation (Figure S4), which was our intention for K-doping. Thus, the remainder of this study is devoted to comparatively investigating pristine and 3% K-doped $LaFeO_3$ electrodes. Hereafter, K-doped $LaFeO_3$ refers to 3% K-doped $LaFeO_3$, unless noted otherwise.

X-ray diffraction (XRD) patterns of the pristine and K-doped $LaFeO_3$ electrodes are shown in Figure 4a. Both

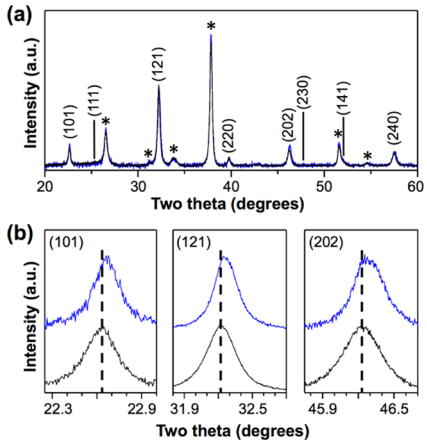

Figure 4. (a) XRD patterns of undoped (black) and 3% K-doped (blue) $LaFeO_3$ films (PDF No: 37-1493). We note that the (*hkl*) indices in PDF 37-1493 are based on the space group *Pnma* (a = 5.5669(4) Å, b = 7.847(7) Å, and c = 5.5530(8) Å). The peaks from the FTO substrate are indicated by an asterisk. (b) Magnification of a few selected (*hkl*) peaks to demonstrate the slight shifts of peaks in two theta values caused by K-doping.

patterns show only the peaks for orthorhombic $LaFeO_3$ (PDF No: 37-1493) except for the peaks from the FTO substrate, confirming the high purity of the pristine and K-doped $LaFeO_3$ samples used in this study. However, the K-doped $LaFeO_3$ electrode shows shifts of all peaks to higher two theta values, as shown by the examples of (101), (121), and (202) peaks (Figure 4b), indicating a decrease in the lattice constants upon K-doping. These results agree well with the computational prediction that the contraction of the unit cell caused by the conversion of Fe^{3+} to Fe^{4+} due to hole-polaron formation outweighs the expansion of the unit cell caused by the replacement of La^{3+} with K^+.

The SEM images of high-surface-area, nanocrystalline pristine and K-doped $LaFeO_3$ electrodes are shown in Figure 5, confirming that these two films have comparable morphologies and surface areas. Thus, any differences in photoelectrochemical properties observed between these two electrodes can be unambiguously attributed to K-doping.

The UV−vis−NIR absorption spectra of pristine and K-doped $LaFeO_3$ are shown in Figure 6a and reveal the difference in photon absorption caused by K-doping. The K-doped sample shows higher absorption below the bandgap transition,

DOI: 10.1021/acs.chemmater.9b02141
Chem. Mater. 2019, 31, 5890−5899

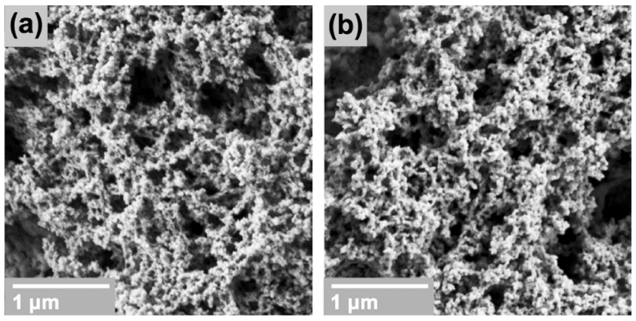

Figure 5. SEM images of (a) pristine and (b) 3% K-doped $LaFeO_3$ films.

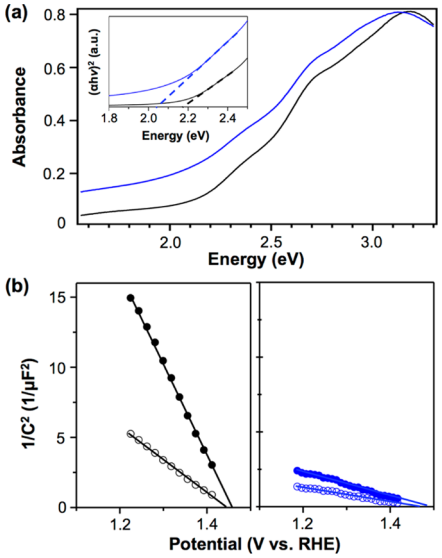

Figure 6. (a) UV−vis−NIR absorption spectra of pristine (black) and 3% K-doped (blue) $LaFeO_3$ electrodes. The inset shows corresponding Tauc plots; (b) Mott−Schottky plots at 0.5 (○) and 1 (●) kHz for pristine (black) and 3% K-doped (blue) $LaFeO_3$ measured in 0.1 M KOH (pH 13).

which was predicted by the computational study, as shown in Figure 3. A more meaningful change in absorbance caused by K-doping, which can contribute to the enhancement of photocurrent, is the decrease in the bandgap energy that allows the bandgap transition to occur at a lower energy. Based on the absorption spectra shown in Figure 6a along with Tauc plots shown in the inset, the bandgap energies of the pristine and K-doped $LaFeO_3$ samples were estimated to be ∼2.2 and ∼2.0 eV, respectively. The decrease in the bandgap energy caused by K-doping agrees well with the computational results.

The computational study also predicted that K-doping creates shallow acceptor levels and, therefore, can effectively increase the majority carrier concentration. To experimentally confirm this, Mott−Schottky plots of $LaFeO_3$ and K-doped $LaFeO_3$ were obtained in a 0.1 M KOH solution (pH 13) at two different frequencies (Figure 6b). The Mott−Schottky plots we obtained for both samples showed some frequency dependence in their slopes. Also, the exact surface areas of these electrodes are unknown. Therefore, accurate quantitative values for a majority carrier density of these electrodes could not be determined using the Mott−Schottky plots. However, because the pristine and K-doped electrodes have comparable morphologies and consequently comparable surface areas (Figure 2), a qualitative comparison can still be made by comparing their slopes. Figure 6b shows that the slopes of the K-doped sample are considerably smaller than those of the pristine sample at the corresponding frequency. Therefore, an increase in the majority carrier density caused by K-doping could be clearly confirmed.

Since the computational study predicted that K-doping results in the formation of Fe^{4+} due to the localization of extra holes on Fe^{3+}, we used X-ray photoelectron spectroscopy (XPS) to detect and compare the amount of Fe^{4+} ions present in the pristine and K-doped $LaFeO_3$ samples. The Fe 2p spectra for pristine and K-doped $LaFeO_3$ are shown in Figure 7a, where Fe $2p_{3/2}$ peak at ∼710 eV and its corresponding satellite peak at ∼718 eV, as well as the Fe $2p_{1/2}$ peak at ∼724 eV and its corresponding satellite peak at ∼732 eV, are well-resolved. These peak positions match well with those expected for a compound containing Fe predominantly in the form of Fe^{3+}.[41] To examine the amount of Fe^{4+} present in these samples, we performed a peak fitting of the main Fe $2p_{3/2}$ peak (Figure 7b,c) to deconvolute it to three components: Fe^{2+}, Fe^{3+}, and Fe^{4+} (Table S3).[11,20,42,43] The content of Fe^{4+} in the pristine sample was determined to be 7.7% of the total Fe concentration, which increased to 15.9% Fe^{4+} in the 3% K-doped $LaFeO_3$ film. We note that the presence of Fe^{4+} in the pristine sample is expected, as the pristine sample possesses intrinsic defects such as lanthanum vacancies that can lead to the formation of Fe^{4+}, which is also the reason why pristine $LaFeO_3$ is p-type. The sizeable increase in Fe^{4+} concentration in the K-doped sample over the pristine sample additionally confirms the increase in the majority carrier density by K-doping and the localization of extra holes on Fe ions.

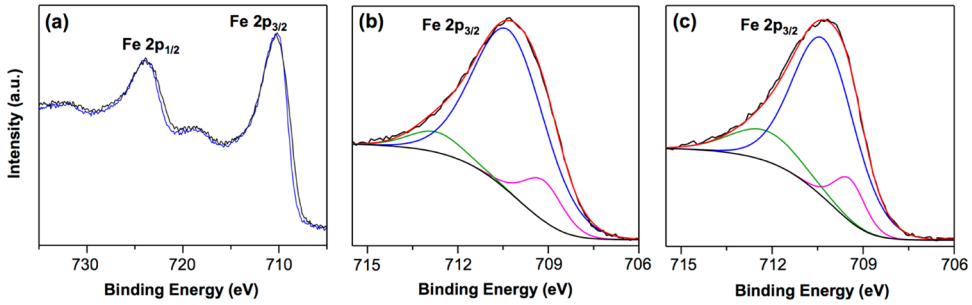

Figure 7. (a) XPS spectra of Fe 2p species at the surface of pristine (black) and 3% K-doped (blue) $LaFeO_3$. Peak fitting of the experimental Fe $2p_{3/2}$ peak (black) with a simulated (red) peak composed of Fe^{4+} (green), Fe^{3+} (blue), and Fe^{2+} (pink) for (b) undoped and (c) 3% K-doped $LaFeO_3$.

DOI: 10.1021/acs.chemmater.9b02141
Chem. Mater. 2019, 31, 5890−5899

The photoelectrochemical properties of pristine and K-doped $LaFeO_3$ were compared for photoreduction of O_2 in O_2-saturated 0.1 M KOH (pH 13) under chopped AM 1.5G 100 mW/cm^2 illumination. $LaFeO_3$ is known to be a good catalyst for the oxygen reduction reaction.[1,11,12] Therefore, photoreduction of O_2 can allow us to directly observe the effect of K-doping on the photoelectrochemical properties without being limited by interfacial charge-transfer kinetics as in the case of photoreduction of water. Figure 8a shows that K-doped

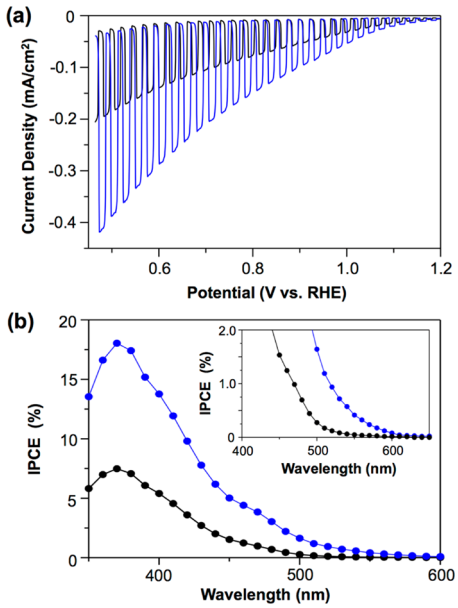

Figure 8. (a) $J-V$ plots (scan rate: 10 mV/s) and (b) IPCE at 0.65 V vs RHE for pristine (black) and 3% K-doped (blue) $LaFeO_3$ for oxygen reduction under AM 1.5G, 100 mW/cm^2 illumination in 0.1 M KOH (pH 13) saturated with O_2.

$LaFeO_3$ significantly increases the photocurrent density over the entire potential range. For example, K-doped $LaFeO_3$ generated a photocurrent density of -268 μA/cm^2 at 0.6 V vs RHE, which was more than double the photocurrent density generated by the pristine $LaFeO_3$ (-124 μA/cm^2) at the same potential. Both samples show nonzero dark current below 1.0 V vs RHE because $LaFeO_3$ is a good electrocatalyst for O_2 reduction and can electrochemically reduce O_2 below 1.0 V vs RHE without light.[1,11]

Our earlier discussion stated that the favorable effect of K-doping is not only an increase in the carrier density but also an increase in the photon absorption owing to the bandgap reduction. To examine whether the enhanced photon absorption caused by K-doping indeed can contribute to photocurrent generation, we obtained incident photon-to-current efficiency (IPCE) of pristine and K-doped samples for O_2 reduction so that their wavelength-dependent photocurrent generation could be compared. Figure 8b shows that in addition to the general increase in IPCE over all wavelengths, which is a result of the enhanced electron–hole separation caused by an increased carrier density, the photocurrent onset for the K-doped sample is clearly shifted from 580 to 640 nm. This shift agrees well with the decrease in the bandgap energy caused by K-doping and confirms that the enhanced photon absorption from the bandgap change directly contributes to the photocurrent enhancement in the K-doped $LaFeO_3$.

In our previous study, a distinct advantage of $LaFeO_3$ as a photocathode was reported to be its photostability; it was stable during photocurrent generation without the need for a protection layer or a catalyst.[1] To confirm that the K-doped samples remained photostable, $J-t$ plots of pristine and K-doped $LaFeO_3$ were measured for O_2 reduction at 0.8 V vs RHE (Figure 9). The results show stable photocurrent generation by both K-doped $LaFeO_3$ and pristine $LaFeO_3$ over 15 h, confirming that K-doping did not alter the photostability of $LaFeO_3$.

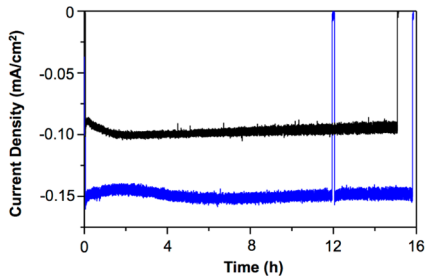

Figure 9. $J-t$ plots at 0.8 V vs RHE for pristine (black) and 3% K-doped (blue) $LaFeO_3$ for oxygen reduction under AM 1.5G, 100 mW/cm^2 illumination in 0.1 M KOH (pH 13) saturated with O_2.

Our previous study showed that the surface of $LaFeO_3$ is not catalytic for water reduction and, therefore, photocurrent that can be generated by $LaFeO_3$ without the addition of a hydrogen evolution catalyst is considerably lower than the photocurrent that $LaFeO_3$ can generate for O_2 reduction due to considerable surface recombination.[1] This means that the effect of K-doping in increasing the number of surface-reaching electrons cannot be fully demonstrated by photocurrent measurements for water reduction. However, we obtained and compared $J-V$ plots of the pristine and K-doped $LaFeO_3$ for water reduction as they can still provide useful information. For this measurement, we used a closed cell containing N_2-purged 0.1 M KOH (pH 13) with a small gas inlet and outlet, which provides a constant flow of N_2 to purge the solution for the duration of the experiment. Because $LaFeO_3$ is catalytic for O_2 reduction, this nearly closed system was required to avoid the introduction of atmospheric O_2 to the electrolyte during photocurrent measurement, which can enhance photocurrent generation. We found that without the use of such a nearly closed system, even if N_2-purged electrolyte is used with constant N_2 purging during the photocurrent measurement, O_2 reduction could not be completely prohibited, resulting in an overestimation of the photocurrent generated for water reduction.

The $J-V$ plots for water reduction shown in Figure 10 show that photocurrent generated by the pristine sample is negligible, as reported in the previous study. The K-doped sample showed only a marginal increase in the steady-state photocurrent because the K-doped $LaFeO_3$ surface is also not catalytic for water reduction. However, the K-doped sample showed a significant increase in transient photocurrent because although the surface-reaching electrons could not be rapidly utilized for water reduction, K-doping increases the number of surface-reaching holes owing to the enhanced photon absorption and bulk electron–hole separation.

Through the combined computational and experimental studies, we showed that K-doping increased the photon absorption and majority carrier density of $LaFeO_3$, which can

DOI: 10.1021/acs.chemmater.9b02141
Chem. Mater. 2019, 31, 5890–5899

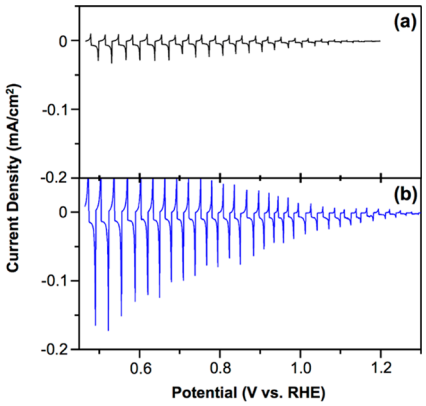

Figure 10. $J-V$ plots for pristine (black) and 3% K-doped (blue) $LaFeO_3$ for water reduction under chopped AM 1.5G, 100 mW/cm^2 illumination in 0.1 M KOH (pH 13) with constant N_2 bubbling (scan rate: 5 mV/s).

effectively increase the number of photoexcited electrons reaching the surface of $LaFeO_3$ under standard solar illumination for use in photoreduction reactions. Our future studies will focus on further improving the photoelectrochemical properties of $LaFeO_3$ by further composition tuning as well as combining $LaFeO_3$ with various H_2 evolution, CO_2 reduction, and N_2 reduction catalysts.

CONCLUSIONS

In summary, we performed a combined theoretical and experimental investigation to examine the effect of substitutional K-doping at the La site (3 atom %) of $LaFeO_3$. The theoretical study showed that K-doping creates shallow acceptor levels above the VBM of $LaFeO_3$ and can effectively increase the majority carrier density. Furthermore, K-doping decreased the bandgap by lowering the CBM and additionally generated multiple highly localized defect states below the CBM. The theoretical study also showed that the two holes generated by the replacement of La^{3+} with K^+ are localized on Fe atoms and their neighboring O atoms, forming Fe^{4+}. The most stable hole-polaron configurations around K were examined. In terms of structure, our theoretical study predicted that K-doping results in a shrinkage of the unit cell owing to the conversion of Fe^{3+} to smaller Fe^{4+} even though K^+ has a larger ionic radius than La^{3+}.

The results obtained from the theoretical studies were verified by experimentally preparing $LaFeO_3$ and K-doped (3 atom %) $LaFeO_3$ as high-quality, high-surface-area electrodes having the same morphology. The XRD patterns indeed showed a decrease in all cell parameters, which confirms the substitution of La^{3+} by K^+ and the resulting Fe^{4+} formation. The increase in Fe^{4+} concentration in K-doped $LaFeO_3$ was also supported by XPS. The UV−vis−NIR absorption spectra showed that K-doping decreased the bandgap by ∼0.2 eV and enhanced the absorption below the bandgap as predicted by the electronic band structure and simulated optical response of K-doped $LaFeO_3$. Furthermore, Mott−Schottky analysis confirmed an increase in the carrier density caused by K-doping. Due to the increase in photon absorption and charge-transport properties, K-doped $LaFeO_3$ generated a significantly increased photocurrent for O_2 reduction, which is a good measure of the increase in the number of surface-reaching electrons under illumination. K-doped $LaFeO_3$ also increased the photocurrent for water reduction. However, the increase in this case was not significant due to the poor catalytic ability of both the pristine and K-doped $LaFeO_3$ for water reduction, resulting in considerable surface recombination. The beneficial effect of the decreased bandgap of K-doped $LaFeO_3$ on photocurrent generation was confirmed by IPCE, which showed photocurrent generation below the bandgap of the pristine $LaFeO_3$. The enhanced photocurrent caused by K-doping was also confirmed to be stable. This study demonstrated that substitutional doping of La^{3+} with K^+ offers an effective way to increase both photon absorption and charge-transport properties that directly influence photocurrent generation by $LaFeO_3$. We plan to perform further investigations of doping at the Fe site as well as doping at the La site with other dopants that vary in nature (alkaline, alkaline earth, or transition metals) and valency to obtain a comprehensive understanding of the effect of composition tuning of p-type oxides with a perovskite structure.

ASSOCIATED CONTENT

Supporting Information

The Supporting Information is available free of charge on the ACS Publications website at DOI: 10.1021/acs.chemmater.9b02141.

Additional electronic band structures, SEM image, and photocurrent measurements; tables showing additional structural data and XPS fitting results (PDF)

AUTHOR INFORMATION

Corresponding Authors

*E-mail: yuanping@ucsc.edu (Y.P.).
*E-mail: kschoi@chem.wisc.edu (K.-S.C.).

ORCID

Yuan Ping: 0000-0002-0123-3389
Kyoung-Shin Choi: 0000-0003-1945-8794

Author Contributions

‖G.P.W. and V.U.B. contributed equally to this work.

Notes

The authors declare no competing financial interest.

ACKNOWLEDGMENTS

K.-S.C. acknowledges financial support for the experimental work by the Division of Chemical Sciences, Geosciences, and Biosciences, Office of Basic Energy Sciences of the U.S. Department of Energy through Grant DE-SC0008707. Y.P. acknowledges financial support for the computational work from the National Science Foundation under grant no. DMR-1760260 and CHE-1904547. Y.P. used resources of the Center for Functional Nanomaterials, which is a U.S. DOE Office of Science Facility, and the Scientific Data and Computing Center, a component of the Computational Science Initiative, at Brookhaven National Laboratory under Contract No. DE-SC0012704. Y.P. also used the Extreme Science and Engineering Discovery Environment (XSEDE),[44] which is supported by National Science Foundation grant number ACI1548562.

REFERENCES

(1) Wheeler, G. P.; Choi, K.-S. Photoelectrochemical Properties and Stability of Nanoporous p-Type $LaFeO_3$ Photoelectrodes Prepared by Electrodeposition. *ACS Energy Lett.* **2017**, *2*, 2378−2382.

DOI: 10.1021/acs.chemmater.9b02141
Chem. Mater. 2019, 31, 5890−5899

(2) Yu, Q.; Meng, X. G.; Wang, T.; Li, P.; Liu, L. Q.; Chang, K.; Liu, G. G.; Ye, J. H. A Highly Durable p-$LaFeO_3$/n-Fe_2O_3 Photocell for Effective Water Splitting Under Visible Light. *Chem. Commun.* **2015**, *51*, 3630−3633.
(3) Parida, K. M.; Reddy, K. H.; Martha, S.; Das, D. P.; Biswal, N. Fabrication of Nanocrystalline $LaFeO_3$: An Efficient Sol-Gel Auto-Combustion Assisted Visible Light Responsive Photocatalyst for Water Decomposition. *Int. J. Hydrogen Energy* **2010**, *35*, 12161−12168.
(4) Tijare, S. N.; Joshi, M. V.; Padole, P. S.; Mangrulkar, P. A.; Rayalu, S. S.; Labhsetwar, N. K. Photocatalytic Hydrogen Generation Through Water Splitting on Nano-Crystalline $LaFeO_3$ Perovskite. *Int. J. Hydrogen Energy* **2012**, *37*, 10451−10456.
(5) Kang, D.; Hill, J. C.; Park, Y.; Choi, K.-S. Photoelectrochemical Properties and Photostabilities of High Surface Area $CuBi_2O_4$ and Ag-Doped $CuBi_2O_4$ Photocathodes. *Chem. Mater.* **2016**, *28*, 4331−4340.
(6) Paracchino, A.; Laporte, V.; Sivula, K.; Gratzel, M.; Thimsen, E. Highly Active Oxide Photocathode for Photoelectrochemical Water Reduction. *Nat. Mater.* **2011**, *10*, 456−461.
(7) Cardiel, A. C.; McDonald, K. J.; Choi, K.-S. Electrochemical Growth of Copper Hydroxy Double Salt Films and Their Conversion to Nanostructured p-Type CuO Photocathodes. *Langmuir* **2017**, *33*, 9262−9270.
(8) Septina, W.; Prabhakar, R. R.; Wick, R.; Moehl, T.; Tilley, S. D. Stabilized Solar Hydrogen Production with CuO/CdS Heterojunction Thin Film Photocathodes. *Chem. Mater.* **2017**, *29*, 1735−1743.
(9) Díez-García, M.; Gomez, R. Metal Doping to Enhance the Photoelectrochemical Behavior of $LaFeO_3$ Photocathodes. *ChemSusChem* **2017**, *10*, 2457−2463.
(10) Celorrio, V.; Bradley, K.; Weber, O. J.; Hall, S. R.; Fermin, D. J. Photoelectrochemical Properties of $LaFeO_3$ Nanoparticles. *ChemElectroChem* **2014**, *1*, 1667−1671.
(11) Zhu, Y. L.; Zhou, W.; Yu, J.; Chen, Y. B.; Liu, M. L.; Shao, Z. P. Enhancing Electrocatalytic Activity of Perovskite Oxides by Tuning Cation Deficiency for Oxygen Reduction and Evolution Reactions. *Chem. Mater.* **2016**, *28*, 1691−1697.
(12) Sunarso, J.; Torriero, A. A. J.; Zhou, W.; Howlett, P. C.; Forsyth, M. Oxygen Reduction Reaction Activity of La-Based Perovskite Oxides in Alkaline Medium: A Thin-Film Rotating Ring-Disk Electrode Study. *J. Phys. Chem. C* **2012**, *116*, 5827−5834.
(13) Lee, D. K.; Lee, D.; Lumley, M. A.; Choi, K.-S. Progress on ternary oxide-based photoanodes for use in photoelectrochemical cells for solar water splitting. *Chem. Soc. Rev.* **2019**, *48*, 2126−2157.
(14) The American Society for Testing and Materials (ASTM) G-173 spectra. https://www.nrel.gov/grid/solar-resource/spectra-am1.5.html.
(15) Smart, T. J.; Cardiel, A. C.; Wu, F.; Choi, K.-S.; Ping, Y. Mechanistic Insights of Enhanced Spin Polaron Conduction in Cu through Atomic Doping. *npj Comput. Mater.* **2018**, *4*, No. 61.
(16) Park, Y.; Kang, D.; Choi, K.-S. Marked Enhancement in Electron-Hole Separation Achieved in the Low Bias Region by Electrochemically Prepared Mo-Doped $BiVO_4$ Photoanodes. *Phys. Chem. Chem. Phys.* **2014**, *16*, 1238−1246.
(17) Erri, P.; Dinka, P.; Varma, A. Novel Perovskite-Based Catalysts for Autothermal JP-8 Fuel Reforming. *Chem. Eng. Sci.* **2006**, *61*, 5328−5333.
(18) Kuhn, J. N.; Ozkan, U. S. Surface Properties of Sr- and Co-doped $LaFeO_3$. *J. Catal.* **2008**, *253*, 200−211.
(19) Søgaard, M.; Hendriksen, P. V.; Mogensen, M. Oxygen Nonstoichiometry and Transport Properties of Strontium Substituted Lanthanum Ferrite. *J. Solid State Chem.* **2007**, *180*, 1489−1503.
(20) Shi, C. M.; Qin, H. W.; Zhao, M.; Wang, X. F.; Li, L.; Hu, J. F. Investigation on Electrical Transport, CO Sensing Characteristics and Mechanism for Nanocrystalline $La_{1-x}Ca_xFeO_3$ sensors. *Sens. Actuators, B* **2014**, *190*, 25−31.
(21) Giannozzi, P.; Baroni, S.; Bonini, N.; Calandra, M.; Car, R.; Cavazzoni, C.; Ceresoli, D.; Chiarotti, G. L.; Cococcioni, M.; Dabo, I.; Dal Corso, A.; de Gironcoli, S.; Fabris, S.; Fratesi, G.; Gebauer, R.; Gerstmann, U.; Gougoussis, C.; Kokalj, A.; Lazzeri, M.; Martin-Samos, L.; Marzari, N.; Mauri, F.; Mazzarello, R.; Paolini, S.; Pasquarello, A.; Paulatto, L.; Sbraccia, C.; Scandolo, S.; Sclauzero, G.; Seitsonen, A. P.; Smogunov, A.; Umari, P.; Wentzcovitch, R. M. QUANTUM ESPRESSO: A Modular and Open-Source Software Project for Quantum Simulations of Materials. *J. Phys.: Condens. Matter* **2009**, *21*, No. 395502.
(22) Hamann, D. R. Optimized Norm-Conserving Vanderbilt Pseudopotentials. *Phys. Rev. B* **2013**, *88*, No. 085117.
(23) Marini, A.; Hogan, C.; Gruning, M.; Varsano, D. yambo: An Ab Initio Tool for Excited State Calculations. *Comput. Phys. Commun.* **2009**, *180*, 1392−1403.
(24) Jackson, J. D. *Classical Electrodynamics*; John Wiley & Sons, Inc.: NY, 1999.
(25) Govindaraju, G. V.; Wheeler, G. P.; Lee, D.; Choi, K. S. Methods for Electrochemical Synthesis and Photoelectrochemical Characterization for Photoelectrodes. *Chem. Mater.* **2017**, *29*, 355−370.
(26) Kang, D.; Kim, T. W.; Kubota, S.; Cardiel, A.; Cha, H. G.; Choi, K.-S. Electrochemical Synthesis of Photoelectrodes and Catalysts for Use in Solar Water Splitting. *Chem. Rev.* **2015**, *115*, 12839−12887.
(27) Seo, H.; Ping, Y.; Galli, G. The Role of Point Defects in Enhancing the Conductivity of $BiVO_4$. *Chem. Mater.* **2018**, *30*, 7793−7802.
(28) Smart, T.; Ping, Y. Effect of Defects on the Small Polaron Formation and Transport Properties of Hematite from First-Principles Calculations. *J. Phys.: Condens. Matter* **2017**, *29*, No. 394006.
(29) Wu, F.; Ping, Y. Combining Landau-Zener Theory and Kinetic Monte Carlo Sampling for Small Polaron Mobility of Doped $BiVO_4$ from First-Principles. *J. Mater. Chem. A* **2018**, *6*, 20025−20036.
(30) Zhu, Z.; Peelaers, H.; Van de Walle, C. G. Electronic and Protonic Conduction in $LaFeO_3$. *J. Mater. Chem. A* **2017**, *5*, 15367−15379.
(31) Idrees, M.; Nadeem, M.; Atif, M.; Siddique, M.; Mehmood, M.; Hassan, M. M. Origin of Colossal Dielectric Response in $LaFeO_3$. *Acta Mater.* **2011**, *59*, 1338−1345.
(32) Mizusaki, J.; Sasamoto, T.; Cannon, W. R.; Bowen, H. K. Electronic Conductivity, Seebeck Coefficient, And Defect Structure of $LaFeO_3$. *J. Am. Ceram. Soc.* **1982**, *65*, 363−368.
(33) Kim, T.; Ping, Y.; Galli, G.; Choi, K.-S. Simultaneous Enhancements in Photon Absorption and Charge Transport of Bismuth Vanadate Photoanodes For Solar Water Splitting. *Nat. Commun.* **2015**, *6*, No. 8769.
(34) Ping, Y.; Rocca, D.; Galli, G. Optical Properties of Tungsten Trioxide from First-Principles Calculations. *Phys. Rev. B* **2013**, *87*, No. 165203.
(35) Ping, Y.; Galli, G. Optimizing the Band Edges of Tungsten Trioxide for Water Oxidation: A First-Principles Study. *J. Phys. Chem. C* **2014**, *118*, 6019−6028.
(36) Sundararaman, R.; Ping, Y. First-Principles Electrostatic Potentials for Reliable Alignment at Interfaces and Defects. *J. Chem. Phys.* **2017**, *146*, No. 104109.
(37) Smart, T. J.; Wu, F.; Govoni, M.; Ping, Y. Fundamental Principles for Calculating Charged Defect Ionization Energies in Ultrathin Two-Dimensional Materials. *Phys. Rev. Mater.* **2018**, *2*, No. 124002.
(38) Wu, F.; Galatas, A.; Sundararaman, R.; Rocca, D.; Ping, Y. First-Principles Engineering of Charged Defects for Two-Dimensional Quantum Technologies. *Phys. Rev. Mater.* **2017**, *1*, No. 071001.
(39) Beausoleil, G. L.; Price, P.; Thomsen, D.; Punnoose, A.; Ubic, R.; Misture, S.; Butt, D. P. Thermal Expansion of Alkaline-Doped Lanthanum Ferrite Near the Neel Temperature. *J. Am. Ceram. Soc.* **2014**, *97*, 228−234.
(40) Shannon, R. D. Revised Effective Ionic-Radii and Systematic Studies of Interatomic Distances in Halides and Chalcogenides. *Acta Crystallogr., Sect. A: Cryst. Phys., Diffr., Theor. Gen. Crystallogr.* **1976**, *32*, 751−767.

DOI: 10.1021/acs.chemmater.9b02141
Chem. Mater. 2019, 31, 5890−5899

(41) Caronna, T.; Fontana, F.; Natali Sora, I.; Pelosato, R. Chemical Synthesis and Structural Characterization of the Substitution Compound $LaFe_{1-x}Cu_xO_3$ (x=0-0.40). *Mater. Chem. Phys.* **2009**, *116*, 645−648.
(42) Wilson, D.; Langell, M. A. XPS Analysis of Oleylamine/Oleic Acid Capped Fe_3O_4 Nanoparticles as a Function of Temperature. *Appl. Surf. Sci.* **2014**, *303*, 6−13.
(43) Dhankhar, S.; Gupta, K.; Bhalerao, G.; Shukla, N.; Chandran, M.; Francis, B.; Tiwari, B.; Baskar, K.; Singh, S. Anomalous Room Temperature Magnetoresistance in Brownmillerite $Ca_2Fe_2O_5$. *RSC Adv.* **2015**, *5*, 92549−92553.
(44) Towns, J.; Cockerill, T.; Dahan, M.; Foster, I.; Gaither, K.; Grimshaw, A.; Hazlewood, V.; Lathrop, S.; Lifka, D.; Peterson, G.; Roskies, R.; Scott, J.; Wilkins-Diehr, N. XSEDE: Accelerating Scientific Discovery. *Comput. Sci. Eng.* **2014**, *16*, 62−74.

DOI: 10.1021/acs.chemmater.9b02141
Chem. Mater. 2019, 31, 5890−5899